






Nickel(II) complexes of ONS donor Schiff base ligands: synthesis, combined DFT-experimental characterization, redox, thermal, and in vitro biological investigation

R.C. Maurya, B.A. Malik, J.M. Mir, P.K. Vishwakarma, D.K. Rajak & N. Jain


To cite this article: R.C. Maurya, B.A. Malik, J.M. Mir, P.K. Vishwakarma, D.K. Rajak & N. Jain (2015) Nickel(II) complexes of ONS donor Schiff base ligands: synthesis, combined DFT-experimental characterization, redox, thermal, and in vitro biological investigation, Journal of Coordination Chemistry, 68:16, 2902-2922, DOI: [10.1080/00958972.2015.1064526](https://doi.org/10.1080/00958972.2015.1064526)

To link to this article: <http://dx.doi.org/10.1080/00958972.2015.1064526>

 View supplementary material 

 Accepted author version posted online: 22 Jun 2015.
Published online: 21 Jul 2015.

 Submit your article to this journal 

 Article views: 124

 View related articles 

 View Crossmark data 

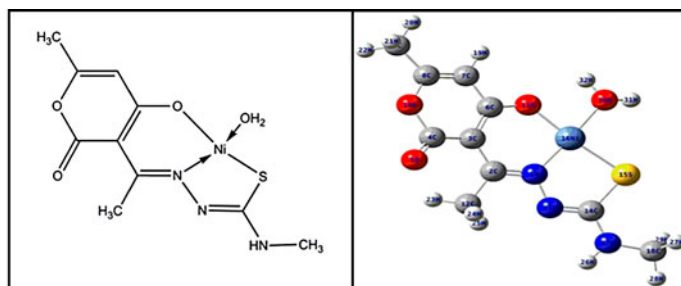
 Citing articles: 1 View citing articles 

Nickel(II) complexes of ONS donor Schiff base ligands: synthesis, combined DFT-experimental characterization, redox, thermal, and *in vitro* biological investigation

R.C. MAURYA*, B.A. MALIK, J.M. MIR, P.K. VISHWAKARMA,
D.K. RAJAK and N. JAIN

Coordination, Bioinorganic and Computational Chemistry Laboratory, Department of P.G. Studies and Research in Chemistry & Pharmacy, R.D. University, Jabalpur, India

(Received 18 December 2014; accepted 29 May 2015)



This article reports the synthesis and characterization of four Ni(II) Schiff base complexes, [Ni(L)(H₂O)], where H₂L = N-(dehydroacetic acid)-thiosemicarbazide (H₂dha-tsc), N-(dehydroacetic acid)-4-methyl-3-thiosemicarbazide (H₂dha-mtsc), N-(dehydroacetic acid)-4-phenyl-3-thiosemicarbazide (H₂dha-ptsc), or N-(dehydroacetic acid)-4-phenylsemicarbazide (H₂dha-psc). The nature of bonding and stereochemistry of these complexes have been deduced from elemental analysis, infrared and electronic spectral studies, molar conductance, magnetic measurements, mass spectrometry, thermogravimetric analysis, ¹H NMR and ¹³C NMR studies, and cyclic voltammetry. The stabilities of the complexes were determined in both solid state and solution. Molecular geometry optimizations and vibrational frequency calculations were performed with Gaussian 09 software package using density functional theory (DFT) with B3LYP/6-311G for a ligand (dha-ptscH₂) and B3LYP/LANL2DZ combination for [Ni(dha-mtsc)(H₂O)]. Based on the combined experimental and theoretical studies, square planar geometry has been proposed for the Ni(II) complexes. The Schiff base ligands and their metal complexes were screened for antibacterial activities against gram-negative bacteria (*Escherichia coli*) at different concentrations to get their minimum inhibition concentration values. The bactericidal activity was enhanced in metal complexes as compared to free ligands.

Keywords: Nickel(II) complexes; Synthesis; Spectroscopic techniques; DFT calculation; Antibacterial

*Corresponding author. Email: rcmaurya1@gmail.com

1. Introduction

The bioinorganic role of nickel has been explored because of the bioavailability of nickel-dependent enzymes including urease, *Escherichia coli* glyoxalase I (*E. coli* Glx I), [NiFe]-hydrogenase, methyl-CoM reductase (MCR), CO dehydrogenase (CODH), and acetyl CoA synthase (ACS), all of which have been crystallographically characterized [1]. The biocatalytic properties of nickel are illustrated by its role in the global carbon cycle and catalysis of the reversible dehydrogenation of CO and H₂O to CO₂ [2]. Superoxide dismutase (SOD) activity has been reported in nickel(II) complexes [3]. Certain nickel(II) thiosemicarbazone Schiff base metal complexes exhibit anti-inflammatory activity by inhibiting NF- κ B transactivation [4]. It has been established that nickel is in thiolate/sulfide environment in the [NiFe]-hydrogenases and in CODH/ACS [5] and hence proves the tendency of nickel to coordinate with sulfur-based scaffolds. Nickel complexes have DNA-binding properties [6], and much effort studies specified amino acid interactions with the metal [7].

Thiosemicarbazones bonding through the nitrogen, sulfur, and oxygen form an important class of biologically active ligands [8], with antitubercular activity, antiviral potential, activity against protozoa small pox, and certain kinds of tumors [9–13]. The chelating properties of thiosemicarbazones have been studied with different metal ions and their complexes with transition and non-transition metals reported [14–18].

Interest has centered on metal complexes of chelating agents containing oxygen, nitrogen, and sulfur donors for the following reasons: (i) Ligands incorporating donors at both medium crystal-field strength (nitrogen donors) and low crystal-field strength (sulfur) might lead to complexes of unusual stereochemistry and with anomalous magnetic and spectroscopic properties; (ii) Biological activities may be expected for some of these compounds. In fact, sulfur–nitrogen ligands and their metal complexes have been reported to possess anti-amoebic [19], antiviral [20], antibacterial [21], antipyretic [22], fungicidal [23], analgesic [22], and cancerostatic activities [24–27]. Ligands containing sulfur as a donor, and the transition metal complexes thereof, have been subject of intense research due to their biological activities [28, 29].

Studies on metal chelates with Schiff bases of dehydroacetic acid [30] play a prominent role in biological applications. Dehydroacetic acid is widely used as fungicide [31] herbicide and as a preservative having powerful anti-microbial effect against bacteria, yeast, and particularly molds [32]. Thermal analysis techniques are used in studying thermal behavior of metal complexes [33–36].

The quantum chemical studies carried out using the density functional theory (DFT) have become an increasingly useful tool for theoretical studies [37–42]. The Cartesian representation of the theoretical force constants are usually computed at optimized geometry by assuming Cs point group symmetry. To show the existence of intramolecular charge transfer (ICT) within molecular systems, the energies of the highest occupied molecular orbital (HOMO) and lowest unoccupied molecular orbital (LUMO) levels and the molecular electrostatic surface potential (MESP) energy surface studies are manipulated by DFT [43].

We have undertaken systematic study of the synthesis and characterization of Ni(II) Schiff base complexes of ligands derived from condensation of dehydroacetic acid and semicarbazone/thiosemicarbazone derivatives (figure 1). Emphasis has been given to comparative DFT-experimental studies of the complexes together with their redox and antibacterial properties.

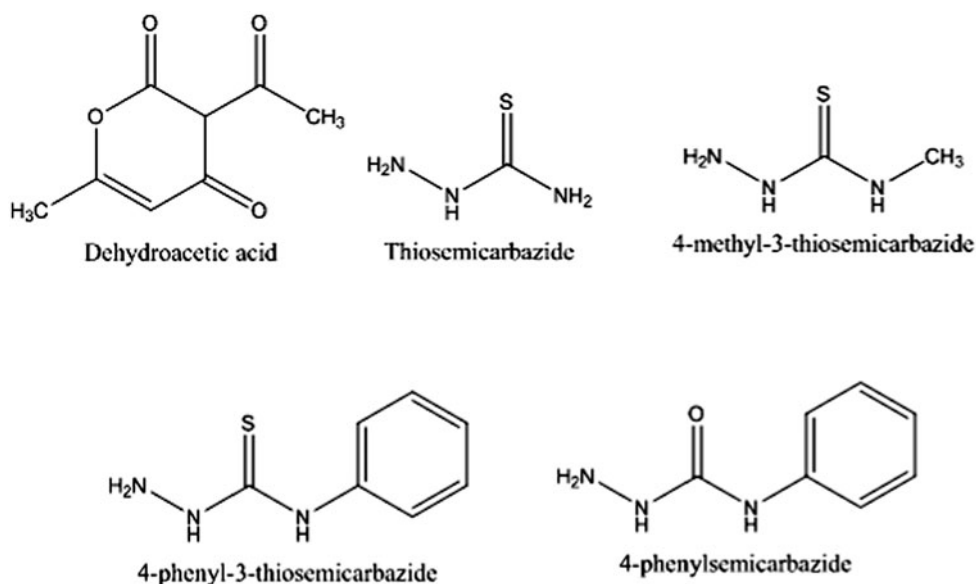


Figure 1. 2D-Structure of organic ligands used for synthesis of Schiff bases.

2. Experimental

2.1. Materials

Dehydroacetic acid was from Merck Specialties Pvt., Ltd., Bombay, semicarbazone and thiosemicarbazone derivatives, *viz.*, thiosemicarbazide, 4-phenyl-3-thiosemicarbazide, 4-methyl-3-thiosemicarbazide, 4-phenyl-semicarbazide were from Aldrich Chemical Co., USA. Nickel(II) chloride hexahydrate was from B.D.H. Chemicals, Mumbai. All other chemicals used were of analytical reagent grade.

2.2. Synthesis of Schiff bases

Schiff bases with semicarbazone and thiosemicarbazone derivatives were prepared as follows: a methanolic solution (10 mL) of dehydroacetic acid (Hdha) (0.168 g, 0.001 mol) was added to the methanolic solution (10 mL) of 4-phenyl-3-thiosemicarbazide (0.167 g, 0.001 mol) (I) or thiosemicarbazide (0.091 g, 0.001 mol) (II) or 4-methyl-3-thiosemicarbazide (0.105 g, 0.001 mol) (III) or 4-phenylsemicarbazide (0.151 g, 0.001 mol) (IV). The resulting solution was refluxed with stirring for 1–2 h at 50–60 °C. The obtained filtrate was concentrated and left overnight at room temperature with solid precipitate of Schiff bases separating from their respective solutions. The obtained precipitate [44] was washed with methanol, recrystallized from ethanol, and dried *in vacuo*.

2.3. Synthesis of nickel(II) complexes

Nickel(II) chloride hexahydrate (0.237 g, 0.001 mol) was dissolved in ethanol (10 mL). Schiff base, 4-phenyl-3-thiosemicarbazide (0.167 g, 0.001 mol) (for **1**) or thiosemicarbazide

(0.091 g, 0.001 mol) (for **2**) or 4-methyl-3-thiosemicarbazide (0.105 g, 0.001 mol) (for **3**) or 4-phenylsemicarbazide (0.151 g, 0.001 mol) (for **4**) was separately dissolved with heating, if required, and stirred in 15 mL of absolute ethanol, containing a few drops of dimethylformamide (DMF). Both the metal salt and Schiff base solutions were mixed, and the resulting solution was refluxed for 5–6 h. The desired compound began to separate out as a fine precipitate keeping the reaction mixture overnight. It was filtered by suction and washed several times with ethanol. All complexes were recrystallized from dichloromethane and then dried *in vacuo* over anhydrous calcium chloride.

2.4. Analysis

- (a) Microanalyses of carbon, hydrogen, and nitrogen of the Schiff bases and complexes were performed on a EURO VECTOR EA 3000 elemental analyzer at CDRI, Lucknow.
- (b) Determination of nickel.

It was estimated as nickel dimethylglyoximate complex by the method reported elsewhere [45].

3. Physical methods

The following physical methods were used to determine the structure of the nickel(II) complexes. ESI mass spectra were recorded on a THERMO Finnigan LCQ advantage max ion trap mass spectrometer at SAIF, CDRI Lucknow. Solid-state infrared spectra were obtained using potassium bromide pellets with a Perkin-Elmer model FT-IR spectrophotometer, in our Department. Conductance measurements were made in DMF solution using a Toshniwal conductivity bridge and dip-type cell with a smooth platinum electrode of cell constant 1.02. Magnetic measurements were performed by Guoy's method using mercury(II)tetrathiocyanatocobaltate(II) as calibrant at SAIF, I.I.T. Bombay. The decomposition temperatures of the complexes were recorded using electrically operated melting point apparatus (Kumar Industries, Mumbai) of heating capacity up to 360 °C. Thermogravimetric analysis was done by heating the sample at 10 °C min⁻¹ from 25 to 1000 °C on a thermal analyzer at SAIF, I.I.T., Bombay. ¹H NMR and ¹³C NMR spectra in DMSO-d₆ were recorded at SAIF, C.D.R.I., Lucknow. Cyclic voltammetric measurements were carried out on an Epsilon (BAS Inc. cell stand) electrochemical system and UV–vis spectra were recorded using a UUV–vis-NIR spectrophotometer (Cary-2005), Agilent Technology, in our Department. Cyclic voltammograms were recorded using a glassy carbon-working electrode, platinum wire auxiliary electrode, and an Ag/AgCl reference electrode. All solutions were purged with N₂ for 30 min before each experiment.

4. Antibacterial assay

The *in vitro* biological screening effects of the investigated compounds were tested against *E. coli* (MTCC 1304) by the well-diffusion method using agar nutrient as the medium and chloramphenicol as standard. The stock solution (1 mg in 1 mL of DMSO) was prepared by

dissolving the compound in DMSO. This solution was serially diluted to find minimum inhibitory concentration (MIC) values (100, 200 $\mu\text{g mL}^{-1}$).

Mueller Hinton agar plates (MHA) were prepared and 50- μL suspensions of microorganism containing approximately 10^5 CFU (colony forming unit) were applied to the plate by the well-diffusion method [46]. The wells were made on the plates and filled with 50 μL of sample solution. These plates were incubated 24 h for bacteria at 37 ± 1 °C. For each sample, the activity was recorded in triplicate. The inhibition zones were taken as average of the triplicates. DMSO was separately tested for the bactericidal properties as blank, and no inhibition zone was found.

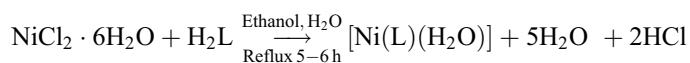
5. Computational methods

To understand the vibrational properties and structural characteristics of the ligands and complexes, the DFT calculations with B3LYP/6-311 + G and B3LYP/LANL2DZ combinations have been used, respectively, and the observed bands are assigned based on the results of normal coordinate analysis. The assignment of the calculated wavenumbers was aided by the animation option of Gauss View 5.0 graphical interface for Gaussian programs, which gives a visual presentation of the shape of the vibrational modes [47, 48]. The Cartesian representation of the theoretical force constants are usually computed at optimized geometry by assuming C_s point group symmetry. The energies of the HOMO and LUMO levels and MESP energy surface studies were used for determining the existence of ICT [43].

To understand the interaction between nickel ion and ONS, *ab initio* total energy calculations within the DFT framework were carried out for $\text{H}_2\text{dha-mtsc}$ ligand and $[\text{Ni}(\text{dha-mtsc})(\text{H}_2\text{O})]$ (3). The optimized structures, vibrational frequencies, HOMO–LUMO, MESP, Mulliken charges, and natural bond orbital (NBOs) charges are discussed. The NMR chemical shifts obtained by applying the gage-including atomic orbital (GIAO) method were computed for such model system. All the theoretical calculations manifested by Gaussian 09 software package [49] were performed at the Department of P.G. Studies and Research in Chemistry and Pharmacy R.D. University Jabalpur, M.P.

6. Results and discussion

The Schiff bases used in the present study were prepared from dehydroacetic acid and thiosemicarbazide and semicarbazide derivatives according to the scheme given in figure 2. The formation of Schiff bases is consistent with the microanalytical data of the ligands. The melting points, colors, yields, and microanalytical data are in Supplementary Information. The formation of the Schiff base ligands is confirmed by the appearance of the azomethine vibration at $1616\text{--}1620\text{ cm}^{-1}$ in the infrared spectra of all the ligands. The nickel(II) complexes were prepared as per the reaction given below.



where $[\text{H}_2\text{L}] = \text{H}_2\text{dha-ptsc}, \text{H}_2\text{dha-tsc}, \text{H}_2\text{dha-mtsc}, \text{H}_2\text{dha-psc}$.

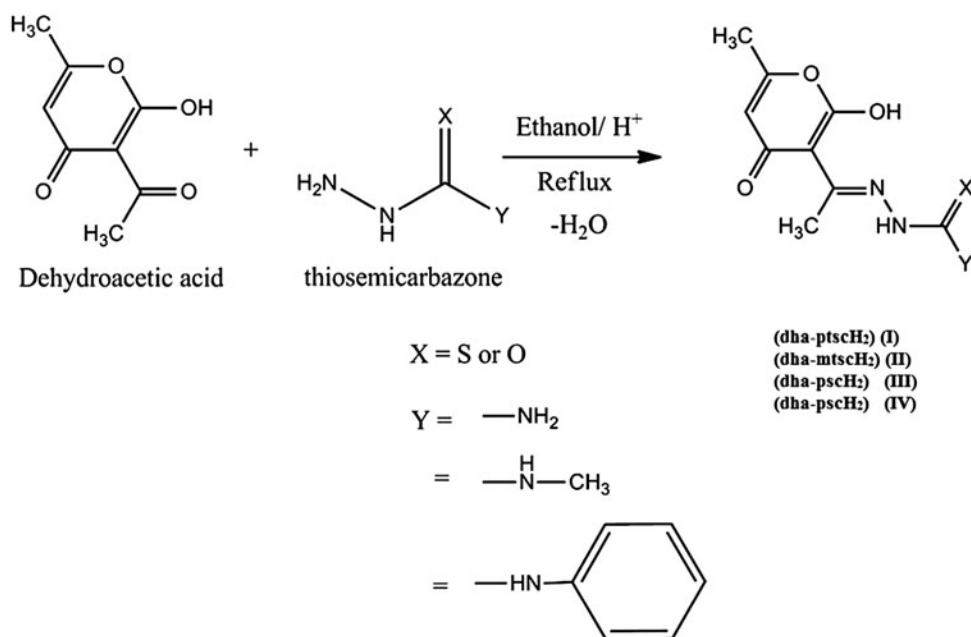


Figure 2. Synthesis of Schiff bases I–IV.

The complexes were air and thermally stable. Their decomposition temperatures and microanalytical data are given in the Supplementary Information. The complexes are insoluble in most solvents but are soluble in DMF and DMSO. The formulation of these complexes has been discussed based on their physicochemical and theoretical studies.

6.1. Conductance measurements

The observed molar conductance ($14.2\text{--}15.6 \text{ Ohm}^{-1} \text{ cm}^2 \text{ mol}^{-1}$) in 10^{-3} M DMSO solutions of these complexes is given in the Supplementary Information and is consistent with the non-electrolytic nature of the complexes [50]. Such a nonzero molar conductance value for each complex in this study is probably due to the strong donor capacity of DMSO, which may lead to displacement of anionic ligand and change of electrolyte type.

6.2. Magnetic measurements

The observed magnetic moments of the synthesized complexes are given in the Supplementary Information. The magnetic measurements indicate that all complexes are diamagnetic [51].

6.3. Infrared spectral studies

All ligands used in this study exist in *enol* and *thiol* form (vide supra) as shown in the Supplementary Information. They possess potential donor sites of three hydrazine nitrogen N₁, N₂, and N₄ (see Supplementary Information) of thiosemicarbazide, *thione/thiolic* sulfur,

enolic oxygen of dhaH, and pyran carbonyl oxygen of Hdha. Considering the planarity of the ligands, coordination of pyrane C=O is unlikely due to being at the back side of the suitable donor sites. It has also been confirmed by the existence of the peak at 1712 cm^{-1} both in the ligand and the complex. Coordination of N_2 and N_4 will be less favored in the presence of neighboring azomethine nitrogen, N_1 and *thiolic* S/enolic O which will form a five-membered chelate ring including nickel after complexation. Both N–N and N–H frequencies remained unaltered on complexation, proving their inertness towards coordination to metal as revealed by no change in $\nu(\text{N–N})$ ($950\text{--}960\text{ cm}^{-1}$) and $\nu(\text{N–H})$ (3150 cm^{-1}) of the free ligands after complexation.

The IR spectrum of all ligands showed a sharp peak at $1614\text{--}1620\text{ cm}^{-1}$ corresponding to $\nu(\text{C=N})$ of the azomethine group. In IR spectra of the complexes, this band shifted to lower energy at $1599\text{--}1606\text{ cm}^{-1}$ indicating coordination of azomethine nitrogen [52]. The coordination of *thiolic* S is confirmed by the downward shift of $\nu(\text{C–S})$ from $814\text{--}817\text{ cm}^{-1}$ in the ligands (I), (II), and (III) to $781\text{--}785\text{ cm}^{-1}$ in **1–3** [53, 54].

The characteristic enolic $\nu(\text{OH})$ mode in the ligands due to the presence of a hydroxyl group was observed at $3430\text{--}3448\text{ cm}^{-1}$. A medium band at $1460\text{--}1468\text{ cm}^{-1}$ due to $\nu(\text{C–O})$ of the enolic group was also observed in these ligands. The band due to enolic $\nu(\text{OH})$ of these ligands was absent in the complexes indicating coordination of the enolic oxygen, after deprotonation. Such coordination is supported by the shifting of the enolic $\nu(\text{C–O})$ band to lower wavenumber, at $1420\text{--}1425\text{ cm}^{-1}$ in the complexes. The presence of coordinated water in all compounds is revealed by the presence of weak bands at 3385 and 3460 cm^{-1} . The appearances of new bands at $430\text{--}441\text{ cm}^{-1}$ are due to the $\nu(\text{Ni–N})$.

Important infrared spectral bands of the ligands and complexes along with their tentative assignments are given in tables 1 and 2. The experimental IR spectra of $\text{H}_2\text{dha-mtsc}$ and $[\text{Ni}(\text{dha-mtsc})(\text{H}_2\text{O})]$ (**3**) are given in the Supplementary Information. The DFT-based IR spectrum of $[\text{Ni}(\text{dha-mtsc})(\text{H}_2\text{O})]$ (**3**) shows close resemblance with the important spectral bands with that of corresponding experimental spectral bands as shown in the Supplementary Information.

6.4. Electronic spectral insights

The solution and solid-state electronic spectra of $[\text{Ni}(\text{dha-mtsc})(\text{H}_2\text{O})]$ (**3**) and $[\text{Ni}(\text{dha-ptsc})(\text{H}_2\text{O})]$ (**1**) are given in the Supplementary Information. UV–vis spectra of the representative Ni(II) complexes in the solid state as well as in their DMSO solution were measured from 200 to 800 nm. Two main spectral bands were observed at 260 nm and 370–378 nm in solution spectra of the complexes. Similar spectral bands were observed at 220 nm and 350–378 nm in the solid phase spectra of the two complexes. For recording solid-state spectra, BaSO_4 was taken as a reference. The former band in all spectra is from electronic transition within the ligand, while the latter can be assigned to a weak ligand-to-metal

Table 1. Important IR bands observed in spectra of the Schiff bases.

Schiff bases	$\nu(\text{C–O})_{\text{enolic}}$	$\nu(\text{C=N})$	$\nu(\text{OH})$	$\nu(\text{N–H})$	$\nu(\text{C=S})$	$\nu(\text{C=O})_{\text{lactone}}$
$\text{H}_2\text{dha-ptsc}$, I	1464	1616	3445	3150	814	1710
$\text{H}_2\text{dha-tsc}$, II	1466	1614	3430	3151	815	1715
$\text{H}_2\text{dha-mtsc}$, III	1460	1616	3448	3155	817	1716
$\text{H}_2\text{dha-psc}$, IV	1468	1620	3433	3152	–	1713

Table 2. Important IR bands observed in spectra of 1–4.

Compounds	$\nu(\text{C}=\text{N})$ (azomethine)	$\nu(\text{C}-\text{O})$ (enolic)	$\nu(\text{C}-\text{S})$	$\nu(\text{H}_2\text{O})$	$\nu(\text{Ni}-\text{N})$	$\nu(\text{C}=\text{O})$ (lactone)
[Ni(dha-ptsc)(H ₂ O)] (1)	1602	1424	780	3395	432	1715
[Ni(dha-tsc)(H ₂ O)] (2)	1606	1420	785	3390	433	1717
[Ni(dha-mtsc)(H ₂ O)] (3)	1604	1423	781	3385	430	1714
[Ni(dha-psc)(H ₂ O)] (4)	1599	1425	–	3460	441	1713

charge-transfer transition. The absence of square planar d-d spectral bands is probably because they are under the tail of the more intense ligand-to-metal charge-transfer bands. The occurrence of two spectral bands in both the solid states and solution of the compounds is in agreement with the results reported for square planar Ni(II) complexes [55, 56].

6.5. ¹H NMR spectral studies

The ¹H NMR spectra of H₂mtsc-dha and [Ni(mtsc-dha)(H₂O)] were recorded in DMSO-d₆ (Supplementary Information). The ¹H NMR spectrum of the ligand (H₂mtsc-dha) shows a single signal for –NH at $\delta = 11.27$ ppm, while the –CH₃ protons of azomethine carbon are at 2.21 ppm. The proton of SH is at $\delta = 1.23$ ppm [57]. The enolic-OH of Hdha is at 14.01 ppm and disappears in **3** because of coordination of enolic oxygen after deprotonation. The absence of SH proton signal in **3** indicates coordination of thiolic S after deprotonation [58], in agreement with the IR spectral results, related to coordination of the ligands. The phenyl protons at $\delta = 7.01$ – 7.80 ppm remain unchanged in the complexes. The chemical shifts of CH₃C=N shift upfield from 2.2 to 2.4 ppm, clearly showing coordination of azomethine nitrogen. The proton at $\delta = 2.50$ ppm is probably due to DMSO-d₆. Coordinated water in **2** showed characteristic signal around $\delta = 3.3$ ppm, typical for DMSO-d₆ as solvent.

6.6. ¹³C NMR spectral studies

The ¹³C NMR spectra of Schiff base H₂mtsc-dha and **3** in DMSO (Supplementary Information) showed the signals at 180 ppm due to C–S carbon and $\delta = 173$ ppm for C=N carbon of the ligand [58]. After complexation, the carbon signal of C–S shifted to 171 ppm and the chemical shift of C=N shifted to 162 ppm in its complex. The signals at 115–155 ppm due to the heteroaromatic and aromatic carbons of the ligand remain unchanged in **3** [59]. A pentet for DMSO is found at $\delta = 38$ ppm.

6.7. Mass spectra

The electron spray ionization (ESI) mass spectrum of **3** (figure 3) showed peaks at 316, 330, and 332 *m/z* due to the following ion fragments: The peaks at 330 and 332 *m/z* in the mass spectrum quoted are both due to [NiL·H₂O + H]⁺. The 314 and 316 *m/z* peaks may be referred for [NiL·H₂O·CH₂ + H]⁺. Peaks at 257 and 339 *m/z* could not be correlated separately. From the overall mass fragmentations, the results are consistent with the proposed molecular composition of **3**.

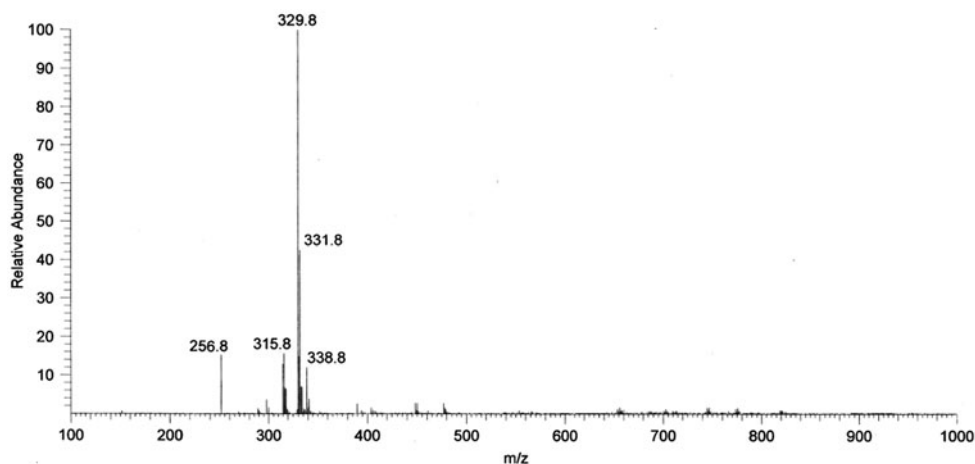


Figure 3. ESI mass spectrum of [Ni(dha-mtsc)(H₂O)] (3).

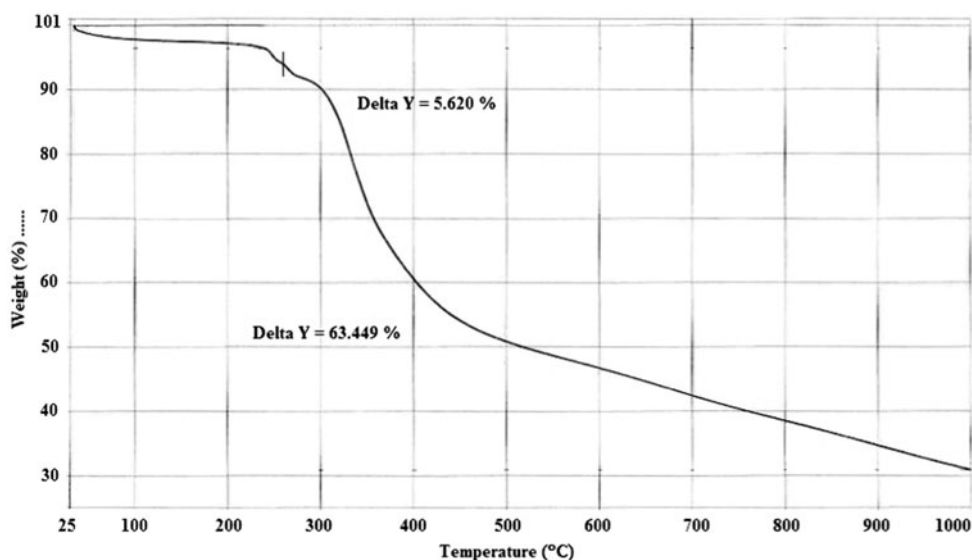


Figure 4. TG curve of 3.

6.8. Thermal analysis

Thermogravimetric analysis of 3 was carried out (figure 4) from 30 to 1000 °C with a heating rate of 10 °C/min. Compound 3 exhibits a weight loss of 5.620% from 30 to 260 °C (Calcd weight loss for 1 mol of H₂O: 5.471%) corresponding to elimination of one molecule of coordinated water. The second weight loss at 260–1000 °C is 63.44% against a calculated weight loss of 64.74% corresponding to elimination of ligand moiety. The final residue (observed 30%) over 1000 °C roughly corresponds to NiO₂ (Calcd 27.05%). These results are consistent with IR results for this complex.

6.9. Electrochemical properties

The redox properties of **3** have been studied using cyclic voltammetry to assess electron transfer reactions. The complexes were dissolved in DMSO, and the cyclic voltammograms were recorded from +1500 to -1500 mV in the presence of 0.1 M of tetrabutylammonium perchlorate (TBAP) as a supporting electrolyte.

The Ni(II) complex exhibits one-electron quasi-reversible transfer process with a reduction wave at $E_{pc} = -448$ mV and the corresponding oxidation wave at $E_{pa} = -298$ mV at a scan rate of 100 mV/s (figure 5). The peak separation (ΔE_p) of this couple is 150 mV. With increasing scan rate, ΔE_p increases (table 3) giving further evidence for the quasi-reversible Ni(II)/Ni(I) couple [60, 61]. The difference between forward and backward potentials can provide a rough evaluation of the degree of reversibility. The ratio of cathodic to anodic current was less than one. However, the current increases with increase of the square root of the scan rate. This establishes the electrode process as diffusion controlled.

7. Antibacterial screening

The synthesized ligands and complexes were evaluated for *in vitro* antimicrobial activities against Gram-negative *E. coli* using the well-diffusion method. The MIC values are summarized in table 4, and the photographs of antimicrobial screening result showing zone of inhibition are presented in the Supplementary Information. The data obtained are comparable to the results reported recently for similar complexes [62, 63]. From the antibacterial screening performed by varying concentration, it is evident that the increase of the concentration of the model compounds increases their activity. Hence, this clarifies that the biological activity is concentration dependent. Increase in activity of the Schiff bases in their corresponding metal complexes shows the significance of metal center to design more potent antibiotics.

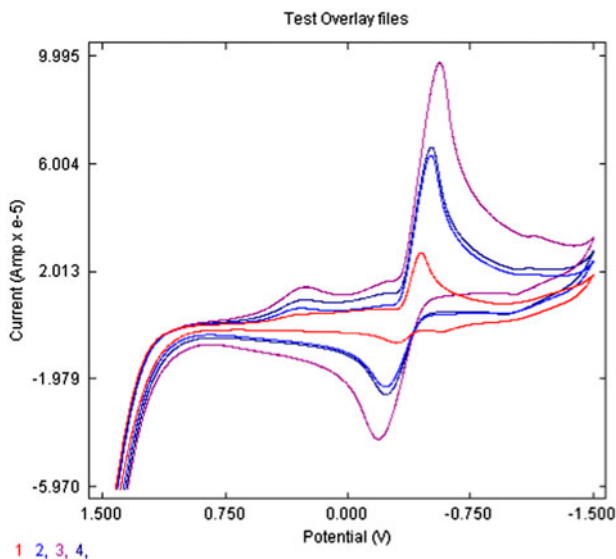


Figure 5. Cyclic voltammograms of **3**.

Table 3. Cyclic voltammetric data for the Ni(II)/Ni(I) couple of **3**.

Scan rate (mV/s)	E_{pc} (mV)	E_{pa} (mV)	E_r (mV)	ΔE (mV)	i_{pc} (μ A)	i_{pa} (μ A)
100	-448.3	-298	-373	150	27.43	-6.84
200	-509.4	-228	-368	281	62.50	-22.54
500	-560.0	-188.6	-374	371	96.7	-43.0

Notes: Supporting electrolyte: tetrabutylammonium tetrafluoroborate, $[\text{CH}_3(\text{CH}_2)_3]_4\text{NBF}_4$ (50 M); concentration of complexes: 1 M; all the potentials are referenced to Ag/AgCl electrode; $E_r = 0.5(E_{pa} + E_{pc})$, where E_{pa} and E_{pc} are anodic and cathodic potentials.

Table 4. *In vitro* antimicrobial activity of compounds and their inhibition zone in mm.

Comps./conc. ($\mu\text{g mL}^{-1}$)	<i>E. coli</i>	
	100	200
(H ₂ dha-ptsc)	16	18
[Ni(dha-ptsc)(H ₂ O)]	24	27
(H ₂ dha-tsc)	15	19
[Ni(dha-tsc)(H ₂ O)]	25	26
(H ₂ dha-mtsc)	17	19
[Ni(dha-mtsc)(H ₂ O)]	23	51
(H ₂ dha-psc)	15	18
[Ni(dha-psc)(H ₂ O)]	25	29
Standard (Chloramphenicol)	30	45

8. Computational studies

8.1. Geometrical parameters

The optimized geometry of both model compounds furnished the total energy E (RB3LYP), -778.86 a.u. or ~ -21194.33 eV for ligand, whereas -1033.42 a.u. or ~ -28121.43 eV was obtained for the complex, reflecting that stability is more in the complex. The various bond lengths, angles, and dihedral angles generated from the optimized structure of **3** using Gaussian 09 software are given in the Supplementary Information and show good resemblance with the X-ray structural investigations of similar complexes previously reported [61]. The computed bond lengths, Ni-S (15), Ni-O(enolic) (11), Ni-N (1), and Ni-O(water) (30), in the present complex are 2.245, 1.849, 1.876, and 1.927 Å, respectively. The computed bond angles in the complex, such as N(1)-Ni(16)-O(11), (95.72°), S(15)-Ni(16)-O(30), (92.48°), N(1)-Ni(16)-S(15), (90.24°), O(11)-Ni(16)-O(30), (81.51°), S(15)-Ni(16)-O(11), (173.79°), N(1)-Ni(16)-O(30), and (177.11°) suggest square planar structure. The optimized structure of **3** is shown in figure 6.

8.2. Frontier molecular orbitals analysis

HOMO and LUMO are very important parameters [64] for chemical reactions. The HOMO is the orbital that primarily acts as an electron donor and the LUMO is the orbital that largely acts as electron acceptor, and the gap between HOMO and LUMO characterizes the molecular chemical stability [65]. Six important molecular orbitals (MOs), third highest [HOMO-2], second highest [HOMO-1], and highest occupied MO's [HOMO], the lowest [LUMO], second lowest [LUMO + 1] and third lowest unoccupied MO's [LUMO + 2] have been worked out for H₂dha-mtsc. The computed energies of these six molecular orbitals are

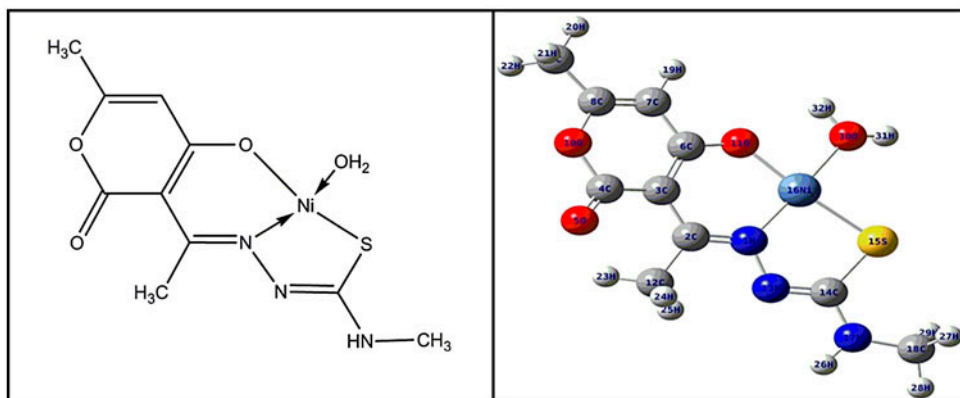


Figure 6. 2D and 3D optimized structure of **3**.

−3.9307, −3.7626, −3.6823, 0.4743, 1.5494, and 2.0379 eV, respectively, and the energy gap (ΔE) between [HOMO – LUMO], [HOMO−1 – LUMO + 1], [HOMO−2 – LUMO + 2] for [H₂dha-mtsc] is 4.1566, 5.3120 and 5.9686 eV, respectively. Similarly six (MO's), viz., [HOMO−2], [HOMO−1], [HOMO], [LUMO], [LUMO + 1], and [LUMO + 2] are worked out for [Ni(dha-mtsc)(H₂O)], and the energies are −6.8405, −6.1425, −3.5726, −1.4803, −0.4495, and −0.4035 eV, respectively, while the energy gap between [HOMO – LUMO], [HOMO−1 – LUMO + 1] and [HOMO−2 – LUMO + 2] are 2.0923, 5.6930, and 6.4369 eV, respectively.

The energy of the frontier orbitals for molecules in terms of ionization energy (IE) and electron affinity (IA) of [H₂dha-mtsc] and its complex from Koopmans's theorem [66] is as follows:

$$-E_{\text{HOMO}} = \text{IE} \quad (1)$$

$$-E_{\text{LUMO}} = \text{EA} \quad (2)$$

The absolute electronegativity (χ_{abs}) and absolute hardness (η) of [H₂dha-mtsc] and its complex calculated using (equation S1, see online supplemental material at <http://dx.doi.org/10.1080/00958972.2015.1064526>) [67] are presented in table 5. Hard molecules have a large HOMO–LUMO gap, and soft molecules have a small HOMO–LUMO gap [68]. The energy gap between HOMO and LUMO in complex as compared to ligands is a key factor to mark the stability difference between the two. The HOMO–LUMO structures with energy level diagram of [H₂dha-mtsc], and its complex are shown in the Supplementary Information.

Other important properties related to the dipole moment and hardness are the electrophilicity index (ω) and the global softness (S) shown in (equation S2) and have been also calculated. The values of ω and S are given in table 5.

8.3. Hyperpolarizability calculations

DFT has been used to calculate the dipole moment (μ), mean polarizability (α), and the total first static hyperpolarizability (β_0) [69, 70] for **3** in terms of x, y, and z components and is

Table 5. Absolute electronegativity (χ_{abs}) and absolute hardness (η) electrophilicity index (ω), global softness (S) of $\text{H}_2\text{dha-mtsc}$ and $[\text{Ni}(\text{dha-mtsc})(\text{H}_2\text{O})]$.

Compound	χ_{abs} (eV)	η (eV)	ω (Debye/eV)	S (eV)	μ (Debye)
$\text{H}_2\text{dha-mtsc}$	-1.6038	-2.0781	-21.14	-0.4812	6.6287
$[\text{Ni}(\text{dha-mtsc})(\text{H}_2\text{O})]$	-2.5263	1.0473	44.021	0.9548	6.7900

given in equation S3. The calculated electric dipole moment μ (Debye), isotropic polarizability (α in a.u.), anisotropy of the polarizability ($\Delta\alpha$ in a.u.), and all hyperpolarizability (β) component (in a.u.) values are given in table 6.

8.4. Atomic net charges

The natural atomic charges of **3** obtained by NBO and Mulliken population analysis [71] with B3LYP/ LANL2DZ basis set are compared in the Supplementary Information. The comparison between Mulliken's net charges and the atomic natural ones is not an easy task since the theoretical backgrounds of the two methods are very different. Looking at the results there are surprising differences between Mulliken's and NBO charges. The data given in the Supplementary Information indicate that C_2 , C_4 , C_6 , C_8 , and all hydrogens bear positive charge both in NBO and Mulliken analyses. Ni_{16} also bears positive charge in NBO analysis as well as in Mulliken analysis. The remaining atoms C_7 , C_9 , C_{12} , C_{14} , C_{18} , N_{13} , N_{17} , S_{15} , and all oxygens O_5 , O_{10} , O_{11} , and O_{30} bear negative charges in both analyses. The color range in the scale of positive and negative charge (a) NBO atomic charges and (b) Mulliken atomic charges of the complex is shown in the Supplementary Information.

The definition of Mulliken's charges is based on population analysis. The Mulliken population analysis provides a partitioning of either the total charge density or an orbital density. The number of the electrons in the molecule (N) is the integral of the charge

Table 6. Calculated components of **3**.

Dipole moment (μ)		Hyperpolarizability (β)	
μ_x	-2.1036	β_{xxx}	-79.20
μ_y	-6.2504	β_{yyy}	-162.77
μ_z	-1.6156	β_{zzz}	2.69
μ_{total}	6.7899	β_{xyy}	-84.26
Polarizability (α)		β_{xxy}	-47.01
α_{xx}	-103.97	β_{xxz}	-14.24
α_{yy}	-109.56	β_{xzz}	-4.06
α_{zz}	-128.67	β_{yzz}	-12.17
α_{xy}	-22.83	β_{yyz}	-19.67
α_{xz}	-1.63	β_{xyz}	-12.70
α_{yz}	-0.56	β_0	279.82
α_{total}	-144.06		
$\Delta\alpha$	22.43		

Notes: α_{xx} , α_{yy} , and α_{zz} are tensor components of polarizability; β_{iiz} , β_{izi} , and β_{zii} (1 from x to z) are tensor components of hyperpolarizability; μ_x , μ_y , and μ_z are the components of the dipole moment. α is the mean polarizability, $\Delta\alpha$ is the anisotropy of polarizability, and β_0 is the mean first hyperpolarizability.

density over the space; N is partitioned for all atoms considering also the overlap population. According to the theory, the overlap population of atoms A and B is divided between the two atoms in half-to-half ratio. This is one weak point of the theory. The other weak point is its strong dependence on the basis set applied. The atomic net charge is the difference between the calculated number of electrons belonging to the atom in the complex and the number of electrons of the isolated atom.

The natural atomic charge is based on the theory of natural population analysis. The analysis is carried out with NBOs. The derivation of a valence-shell atomic orbital (NAO) involves diagonalization of the localized block of the full-density matrix of a given molecule associated with basic functions on that atom. A distinguishing feature of NAOs is that they meet the simultaneous requirement of orthonormality and maximum occupancy. In a polyatomic molecule, the NAOs mostly retain one-center character, and thus, they are optimal for describing the molecular electron density around each atomic center. NBOs are linear combinations of the NAOs of two bonded atoms. The natural population analysis satisfies Pauli's exclusion principle and solves the basis set dependence problem of the Mulliken's population analysis [72].

8.5. Molecular electrostatic potential of ligand and its complex

The Molecular electrostatic potential (MESP) is related to the electron density and is very useful in understanding sites for electrophilic attack and nucleophilic reactions as well as hydrogen-bonding interactions [73–75]. The molecular electrostatic potential, $V(r)$, at a given point $r(x, y, z)$ in the vicinity of a molecule is defined in terms of the interaction energy between the electric charge generated from the molecule's electrons and nuclei and a positive test charge (a proton) located at r . For the system studied, the $V_{(r)}$ values were calculated as described previously using the following equation [76]:

$$V_{(r)} = \sum_A \frac{Z_A}{|R_A - r|} - \int \frac{\rho(r')}{|r' - r|} d^3r' \quad (3)$$

where Z_A is the charge of nucleus A located at R_A , $\rho(r')$ is the electron density function of the molecule, and r' is the dummy integration variable. Being a real physical property, (r) can be determined experimentally by diffraction or by computational methods [77]. To predict reactive sites for electrophilic and nucleophilic attack for the title molecule, MESP was calculated at the 6-311G(+) and LANL2DZ optimized geometries. The negative (red) regions of MESP were related to nucleophilic reactivity, and the positive (blue) regions to electrophilic reactivity are shown in the Supplementary Information.

The MESP surface diagram is used to understand the reactive behavior of a molecule, in that negative regions can be regarded as nucleophilic centers, whereas the positive regions are potential electrophilic sites. The MESP surface displays molecular shape, size and electrostatic potential values of H₂dha-mtsc and [Ni(dha-mtsc)(H₂O)] (**3**). The MESP map of H₂dha-mtsc shows that the thiol group and hydroxyl oxygen represent the most negative potential regions, while in the case of **3**, the coordination environment of four OONS and oxygen (lactonic) is the region of most negative potentials. The hydrogens in H₂dha-mtsc bear the region of maximum positive charge. The two hydrogens attached to the electronegative oxygen of the coordinated water are most electropositive. The predominance of green region in the MESP surfaces corresponds to a potential halfway between the two extremes represented as red and dark blue colors.

8.6. NMR spectral studies

The calculated SCF GIAO magnetic shielding (in solvent phase) and predicted ^1H - and ^{13}C NMR chemical shifts (with respect to TMS, all values in ppm) for **3** optimized by B3LYP/LANL2DZ basis set along with ^1H - and ^{13}C NMR chemical shifts are given in the Supplementary Information along with indexing of proton/carbon signals in different environments. The theoretical assignment of ^1H - and ^{13}C NMR data for **3** is given in table 7. A good agreement has been found between experimental and calculated NMR results.

9. Stability of the synthesized complexes

The combined theoretical and experimental results are evident in declaring that the complexes are quite stable. As discussed earlier, the complexes are colored and are air stable solids. From the theoretical data of frontier orbital analyses and the mode of change in particular bonding sites around the coordination sphere, the complexes have stability. The total computed energy content of the model compounds also depicts the same assumption. Looking at the DFT-based optimized structure of **3** in 1 : 1 and 1 : 2 M ratio of the metal to the ligand, it is apparent that in the former case, the complex acquires square planar geometry and tetrahedral in the latter.

9.1. DFT-based stability insights

The reaction free energy, ΔG , is obtained from DFT calculations of products (1 : 1 and 1 : 2 M ratio of metal to ligand) according to equation

$$\Delta G = G[\text{Ni}(\text{dha} - \text{mtsc})(\text{H}_2\text{O})] - G[\text{Ni}(\text{dha} - \text{mtsc})_2]$$

The potential energy of the solute includes the solute–continuum electrostatic interaction. The term incorporates all non-electrostatic solute–continuum interactions (dispersion and repulsion) plus the cavitation energy resulting from the creation of the vacuum that contains the solute in the dielectric medium. ΔG is the contribution of the vibrational motion of the nuclei to the free energies at 298 K, which is calculated within the harmonic approximation. Comparing the free energy change that the ligand undergoes after complexation for **3** furnishes $\Delta G = -102705.07 \text{ J mol}^{-1}$.

Table 7. Theoretical assignment of ^1H NMR and ^{13}C NMR data for **3** optimized by B3LYP/LANL2DZ basis set.

S. No.	Proton assignment	^1H NMR	Carbon assignment	^{13}C NMR
01	Aromatic Proton	5.77	C–S	185.33
02	–NH	3.72	–C–O (enolic)	184.19
03	N=C–CH ₃	2.10	–C=N–	183.22
04	CH ₃ (mtsc)	1.86–2.02	–C=O (lactone)	182.10
05	CH ₃ -(acetyl of DHA)	1.06–1.45	Aromatic carbons	115.80–118.59
06	–H ₂ O	1.02–1.03	–C=N=CH ₃	35.88

The stability constant (K) of a metal complex is related to the thermodynamic property, free energy change (ΔG) by the usual equation: $\Delta G = -2.303RT \log K$. At room temperature, K is 18.

9.2. Experimental approach

1×10^{-3} M solutions of nickel(II) chloride hexahydrate and N-dehydroacetic acid-4-methyl-3-thiosemicarbazide were prepared separately as stock solutions (100 mL) using three suitable solvents viz., methanol, acetonitrile, and DMSO. 0.5 mL stock solution of nickel(II) chloride hexahydrate in each solvent was pipetted into each of the fifteen test tubes, and aliquots (0, 0.1, 0.2, 0.3, and 0.5 mL) of stock solution of ligand were added. In each test tube of metal–ligand mixture, the total volume was raised to 2 mL by adding the required solvent. The reaction mixtures were shaken. The absorbance of each mixture was taken at λ_{\max} of the complexes in their solvents at room temperature (298 K). The related data are given in table 8 and figure 7.

Using Beer–Lambert's law, we have $A_c = A - [C_{\text{Ni}}(1-x) \cdot b \cdot c]$, where A is uncorrected absorbance and A_c is corrected absorbance for each of the solutions, C_{Ni} = molar absorptivity of Ni, x = mole fraction, b = path length (1 cm), and c = molar concentration (1×10^{-3} M). From the plot obtained for corrected absorbance (A_c) and mole fraction (x) (figure 8), the stoichiometric ratio for the ligand : metal is 1 : 1. The procedure described by Lee *et al.* [78] was also adopted. Job's method of continuous variation was used [79, 80]. The stability constants of metal ions (Ni^{2+}) with the ligand were determined spectrophotometrically using the modified procedure of Hilderbrand and Benesi as described by Rose and Drago [81]. A series of solutions was prepared with a constant concentration of metal ion $[M]$ and variable ligand $[L]$ concentration. The absorbance of each of the mixtures was taken at λ_{\max} previously determined and the stability constant, β , was determined using Hilderbrand and Benesi [82] equation: $M/A = (1/\beta\epsilon_c)(1/L_0) + 1/\epsilon_c$. The plot of M/A versus $1/L$ gives the intercept $1/\epsilon_c$ and slope $1/\beta\epsilon_c$ from which β (stability constant) can be evaluated. The stability constant for the given set of solvents is 30–31, a characteristic feature of

Table 8. UV–vis based stability parameters of **3** using different solvents.

Solvent	Volume of ligand (mL)	Volume of metal salt (mL)	Mole fraction (x) of ligand in 2 mL dilution (L_c)	L_c/M_c ($M_c = 0.25$)	Absorb. (A)	Absorb. correct. (A_c)
Methanol	0	0.5	0	–	1.01	–
Methanol	0.1	0.5	0.05	0.2	1.4	0.44
Methanol	0.2	0.5	0.10	0.4	3.85	2.94
Methanol	0.3	0.5	0.15	0.6	4.57	3.64
Methanol	0.5	0.5	0.25	1	5.40	4.64
DMSO	0	0.5	0	–	1.02	–
DMSO	0.1	0.5	0.05	0.2	2.60	1.63
DMSO	0.2	0.5	0.10	0.4	2.70	1.78
DMSO	0.3	0.5	0.15	0.6	2.99	2.12
DMSO	0.5	0.5	0.25	1	4.43	3.66
Acetonitrile	0	0.5	0	–	1.23	–
Acetonitrile	0.1	0.5	0.05	0.2	1.89	0.72
Acetonitrile	0.2	0.5	0.10	0.4	2.80	1.53
Acetonitrile	0.3	0.5	0.15	0.6	2.01	2.10
Acetonitrile	0.5	0.5	0.25	1	1.07	3.55

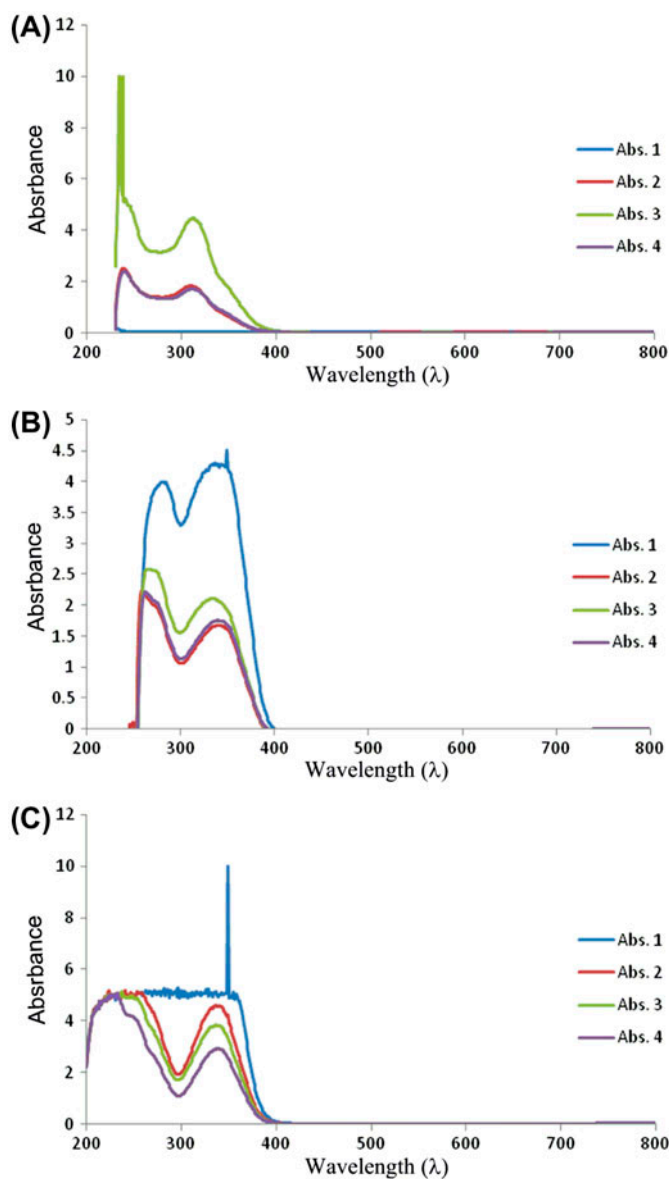


Figure 7. UV-vis spectra of **3** at different dilutions using (A) acetonitrile, (B) DMSO, and (C) methanol as solvents.

square planar nickel(II) complexes. The deviation of stability constant from the theoretical value is due to the computational simulations carried out in gas phase.

In order to prove the same in solution phase, discussed in electronic spectral studies, their colored solutions in DMF and DMSO were left for 72 h to notice any change in their colors, and UV-vis spectra of these solutions were recorded. No noticeable change was

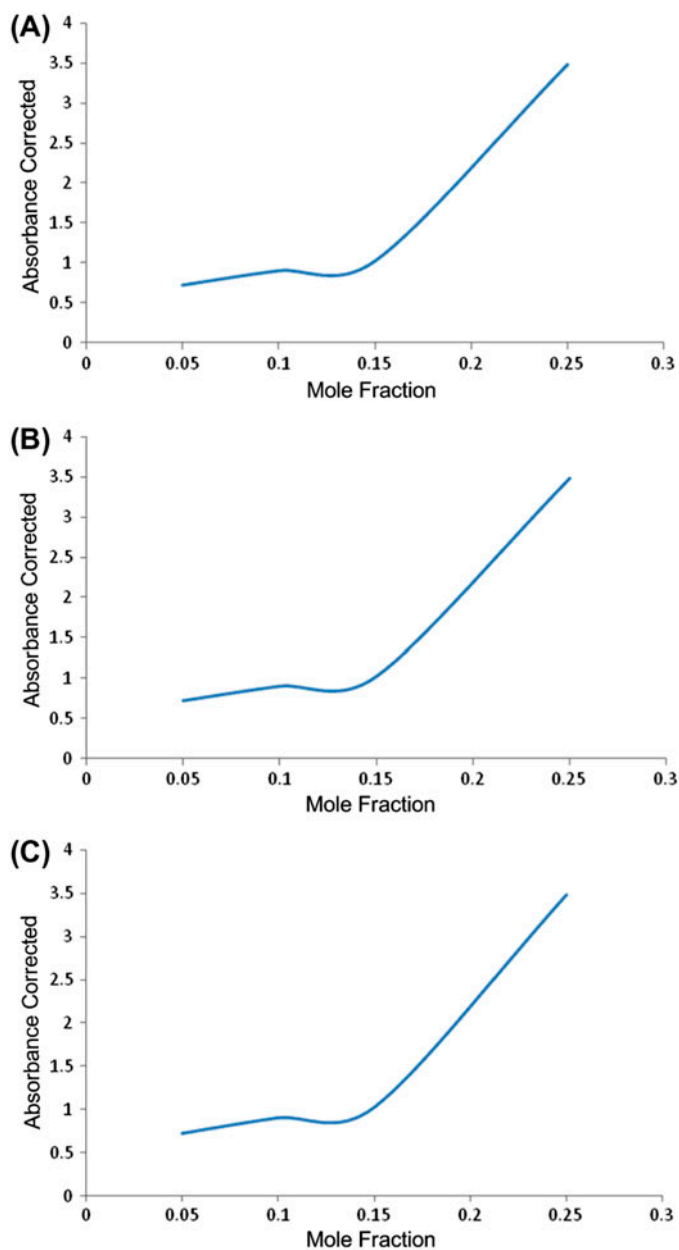
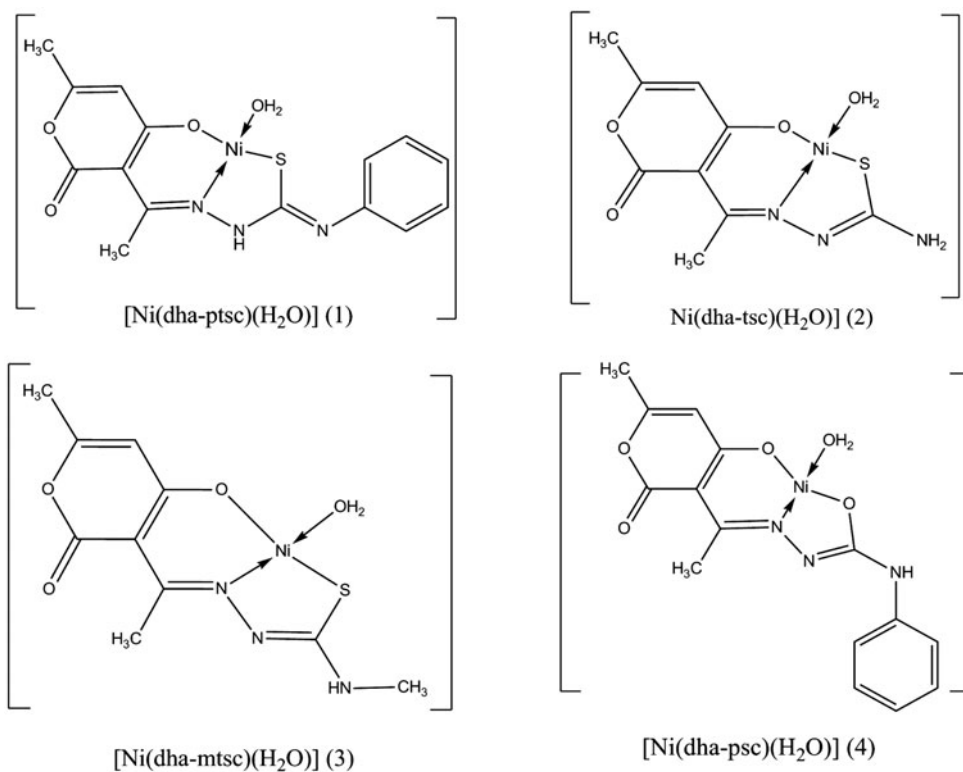


Figure 8. Stoichiometric curves for **3** in (A) methanol, (B) DMSO, and (C) acetonitrile.

detected from their electronic spectra as compared to the spectra recorded for their freshly prepared solutions (Supplementary Information). Hence, from their stability exploration, the complexes under question possess square planar geometry.



Scheme 1. Proposed structure of the complexes.

10. Conclusion

On the basis of physicochemical and computational studies discussed, square planar geometry for Ni(II) complexes is proposed. The ligands are tridentate through carbonyl oxygen, imino nitrogen, and thiolic sulfur. The thermal study of **3** shows that the complex is thermally stable. Scheme 1 shows the proposed structure of the complexes.

The studied complexes represent efficient antimicrobial agents. Investigations regarding their anticancer and DNA linkage behavior may be expected with these compounds. The interesting assets like porosity and solar sensitizing behavior may also be invoked in future investigations.

Acknowledgements

The authors are thankful to UGC for providing grant Gaussian Software 09 through Major Research Project FNo.41-255/2012 (SR). We are thankful to Sophisticated Analytical Instrument Facility, CDRI, Lucknow, India, for Mass, NMR and CHN analysis. Thanks are also due to Sophisticated Analytical Instrument Facility, I.I.T, Mumbai, for TGA and DTA analysis. We also acknowledge the Department of Chemistry and Pharmacy, Rani Durgawati University, Jabalpur for providing laboratory facilities and instruments.

Disclosure statement

No potential conflict of interest was reported by the authors.

References

- [1] F. Meyer, H. Kozłowski. *Comprehensive Coordination Chemistry II*, 6, p. 510, Elsevier, Pergamon (2003). ISBN: 0-08-043748-6.
- [2] H.F. Stanyon, X. Cong, Y. Chen, N. Shahidullah, G. Rossetti, J. Dreyer, G. Papamokos, P. Carloni, J.H. Viles. *FEBS J.*, **281**, 3945 (2014).
- [3] M.M. Ibrahim, G.A.M. Mersal, S.A. Al-Juaid, S.A. El-Shazly. *J. Mol. Struct.*, **1056-1057**, 166 (2014).
- [4] H.B. Shawish, W.Y. Wong, Y.L. Wong, S.W. Loh, C.Y. Looi, P. Hassandarvish, A.Y.L. Phan, W.F. Wong, H. Wang, I.C. Paterson, C.K. Ea, M.R. Mustafa, M.J. Maah. *PLoS ONE*, **9**, e100933 (2014).
- [5] R.M. Evans, F.A. Armstrong. *Metalloproteins*, **1122**, 73 (2014).
- [6] R. Galindo-Murillo, T.E. Cheatham. *Chem. Med. Chem.*, **9**, 1252 (2014).
- [7] M. Can, F.A. Armstrong, S.W. Ragsdale. *Chem. Rev.*, **114**, 4149 (2014).
- [8] B. Pradhan, D.V. Ramana Rao. *J. Ind. Chem. Soc.*, LIV, 136 (1977).
- [9] M. Mohan, P. Sharma, N.K. Jha. *Inorg. Chim. Acta*, **107**, 91 (1985).
- [10] M.B. Belicchi Ferrari, F. Bisceglie, G. Pelosi, P. Tarasconi, R. Albertini, A. Bonati, P. Lunghi, S. Pinelli. *J. Inorg. Biochem.*, **83**, 169 (2001).
- [11] M. Joudel, X.D. Thanh, G. Bouet, S. Bonneau, M.A. Khan. *Anticancer Res.*, **22**, 1713 (2002).
- [12] A. Varshney, J.P. Tandon. *Polyhedron*, **5**, 739 (1986).
- [13] M. Akhtar, D.J. Phillips. *J. Inorg. Nucl. Chem.*, **36**, 22 (1974).
- [14] A.C. Sartorelli, K.C. Agrawal. *Biochem. Pharmacol.*, **20**, 3119 (1971).
- [15] A.J. Lin, K.C. Agrawal, A.C. Sartorelli. *J. Med. Chem.*, **15**, 615 (1972).
- [16] K.N. Thimmaiah, W.D. Lloyd, G.T. Chandrappa. *Inorg. Chim. Acta*, **106**, 81 (1985).
- [17] M. Baldini, M.B. Belicchi-Ferrari, F. Bisceglie, G. Pelosi, S. Pinelli, P. Tarasconi. *Inorg. Chem.*, **42**, 2049 (2003).
- [18] S. Padhye, Z. Afrasiabi, E. Sinn, J. Fok, Kapil Mehta, N. Rath, D. Deobagakar, C.E. Anson, A.K. Powell. *Inorg. Chem.*, **44**, 1154 (2005).
- [19] (a) M.R. Maurya, A. Kumar, A.R. Bhat, A. Bader, C. Rehder. *Inorg. Chem.*, **45**, 1260 (2006); (b) M.R. Maurya, S. Agarwal, M. Abid, A. Azam, C. Bader, M. Ebel, D. Rehder. *Dalton Trans.*, 937 (2006). doi: 10.1039/b512326g.
- [20] Br. Pat. 1045180, 1966 to Parke Davis and Co. see: *Chem. Abstr.*, **66**, 18720g (1967).
- [21] S. Vattum, S. Rao. *Proc. Ind. Acad. Sci.*, **40**, 96 (1959).
- [22] U.S. Pat. 3127410 (Cl. 260-307) to A.E. Wilder Smith. see: *Chem. Abstr.*, **61**, 118g (1964).
- [23] S. Giri, R.K. Khare. *J. Antibact. Antifungal Agents (Jpn.)*, **4**, 11 (1976).
- [24] R.W. Brockaman, J.R. Thomson, M.J. Bell, H.E. Skipper. *Cancer Res.*, **16**, 167 (1956).
- [25] B.L. Frelander, F.A. French. *Cancer Res.*, **18**, 1286 (1958).
- [26] H.G. Petering, H.H. Buskirk, J.A. Crim, G.J. Van Giessen. *Pharmacologist*, **5**, 271 (1963).
- [27] A.M. Evangelou. *Crit. Rev. Oncol. Hematol.*, **42**, 249 (2002).
- [28] (a) M.E. Hossain, M.N. Alam, J. Begum, M. Akbar Ali, M. Nazimuddin, F.E. Smith, R.C. Hynes. *Inorg. Chim. Acta*, **249**, 207 (1996); (b) M.E. Hossain, M.N. Alam, M.A. Ali, M. Nazimuddin, F.E. Smith, R.C. Hynes. *Polyhedron*, **15**, 973 (1996).
- [29] (a) M.A. Ali, A.H. Mirza, A. Monsur, S. Hossain, M. Nazimuddin. *Polyhedron*, **20**, 1045 (2001); (b) M.A. Ali, A.H. Mirza, M. Nazimuddin, P.K. Dhar, R.J. Butcher. *Transition Met. Chem.*, **27**, 27 (2002).
- [30] S. Lui, S.J. Rettig, C. Orvig. *Inorg. Chem.*, **30**, 4915 (1991).
- [31] P.V. Rao, A.V. Narasaih. *Ind. J. Chem.*, **42A**, 1896 (2003).
- [32] M.Z. Chalaca, J.D. Figueroa-Villar, J.A. Ellena, E.E. Castellano. *Inorg. Chim. Acta*, **45**, 328 (2002).
- [33] A.A. Soliman. *J. Therm. Anal. Calorim.*, **63**, 221 (2001).
- [34] G.G. Mohamed, Z.H. Abdel-Wahab. *J. Therm. Anal. Calorim.*, **73**, 347 (2003).
- [35] H.A. El-Borai. *J. Therm. Anal. Calorim.*, **81**, 339 (2005).
- [36] S.H. Patel, P.B. Pansuriya, M.R. Chhasatia, H.M. Parekh, M.N. Patel. *J. Therm. Anal. Calorim.*, **91**, 413 (2008).
- [37] R.C. Maurya, B.A. Malik, J.M. Mir, A.K. Sharma. *J. Coord. Chem.* **67**, 3084 (2014).
- [38] P. Denis, O.N. Ventura. *J. Mol. Struct.*, **537**, 173 (2001).
- [39] A.J. Abbowicz-Bienko, D.C. Bienko, Z. Latajka. *J. Mol. Struct.*, **552**, 165 (2000).
- [40] R. Jacob, G. Fisccker. *J. Mol. Struct.*, **613**, 175 (2002).
- [41] K. Banclersen, M. Langgard, J. Sparget-Larsen. *J. Mol. Struct.*, **509**, 153 (1999).
- [42] Y.Z. Song, J.F. Zhou, Y. Song, Y.G. Wei, H. Wang. *Bioorg. Med. Chem. Lett.*, **15**, 4672 (2005).
- [43] J. Jayabharathi, V. Thanikachalam, M.V. Perumal. *Spectrochim Acta. Part A*, **95**, 614 (2012).

- [44] X. Qiu, J. Wang, D. Shi, S. Li, F. Zhang, F. Zhang, G. Cao, B. Zhai. *J. Coord. Chem.*, **66**, 1616 (2013).
- [45] (a) J. Bassett R.C. Denney, G.H. Jeffery, J. Mendham. *Vogel's Textbook of Quantitative Inorganic Analysis*. ELBS and N. Y. Longman, 5th Edn, Group UK Limited (1978); (b) I.M. Kolthoff, P.J. Eilving. *Treatise on Analytical Chemistry*, Vol. 8, part II, Interscience, New York (1963).
- [46] M.J. Pelczar, E.C.S. Chan, N.R. Krieg. *Text Book of Microbiology*, 5th Edn, p. 138, McGraw-Hill, New Delhi (2001).
- [47] GaussView 9.0, Gaussian Inc., Carnegieoffice. Park, Pittsburgh, PA, USA.
- [48] S. Bayari, S. Saglan, H.F. Ustundag. *J. Mol. Struct: THEOCHEM*, **726**, 225 (2005).
- [49] M.J. Frisch, G.W. Trucks, H.B. Schlegel, G.E. Scuseria, M.A. Robb, J.R. Cheeseman, G. Scalmani, V. Barone, B. Mennucci, G.A. Petersson, H. Nakatsuji, M. Caricato, X. Li, H.P. Hratchian, A.F. Izmaylov, J. Bloino, G. Zheng, J.L. Sonnenberg, M. Hada, M. Ehara, K. Toyota, R. Fukuda, J. Hasegawa, M. Ishida, T. Nakajima, Y. Honda, O. Kitao, H. Nakai, T. Vreven, J.A. Montgomery, Jr., J.E. Peralta, F. Ogliaro, M. Bearpark, J.J. Heyd, E. Brothers, K.N. Kudin, V.N. Staroverov, T. Keith, R. Kobayashi, J. Normand, K. Raghavachari, A. Rendell, J.C. Burant, S.S. Iyengar, J. Tomasi, M. Cossi, N. Rega, J.M. Millam, M. Klene, J.E. Knox, J.B. Cross, V. Bakken, C. Adamo, J. Jaramillo, R. Gomperts, R.E. Stratmann, O. Yazyev, A.J. Austin, R. Cammi, C. Pomelli, J.W. Ochterski, R.L. Martin, K. Morokuma, V.G. Zakrzewski, G.A. Voth, P. Salvador, J.J. Dannenberg, S. Dapprich, A.D. Daniels, O. Farkas, J.B. Foresman, J.V. Ortiz, J. Cioslowski, D.J. Fox, *GAUSSIAN 09* (Revision C.01), Gaussian, Inc., Wallingford, CT (2010).
- [50] W.J. Geary. *Coord. Chem. Rev.*, **7**, 81 (1971).
- [51] J.S. Kumaran, S. Priya, J. Muthukumaran, N. Jayachandramani, S. Mahalakshmi. *J. Chem. Pharm. Res.*, **5**, 56 (2013).
- [52] R.C. Maurya, D.D. Mishra, N.S. Rao, M.N. Jayaswal, N.N. Rao. *Polyhedron*, **12**, 2045 (1993).
- [53] R.C. Maurya, D.D. Mishra, N.S. Rao, N.N. Rao. *Synth. React. Inorg. Met.-Org. Chem.*, **24**, 1013 (1994).
- [54] M. Kalita, P. Gogoi, P. Barman, B. Sarma. *J. Coord. Chem.*, **67**, 2445 (2014).
- [55] M. Baranska, W. Lasocha, H. Kozłowski, L.M. Proniewicz. *J. Inorg. Biochem.*, **98**, 995 (2004).
- [56] S. Celen, E. Gungor, H. Kara, A. Dilek Azaz. *J. Coord. Chem.*, **66**, 3170 (2013).
- [57] S. Kannan, M. Sivagamasundari, R. Ramesh, Y. Liu. *J. Organomet. Chem.*, **693**, 2251 (2008).
- [58] H. Ullah, F.H. Wattoo, M.H.S. Wattoo, M. Gulfranz, S.A. Tirmizi, S. Ata, A. Wadood. *Turk. J. Biochem.*, **37**, 386 (2012).
- [59] N.N. Dzulkifli, Y. Farina, I. Baba, N. Ibrahim. *The Malaysian J. Anal. Sci.*, **16**, 103 (2012).
- [60] J. Bard, L.R. Izatt, *Electrochemical Methods: Fundamentals and Applications*: 2nd Edn, Wiley, New York (2001).
- [61] A.M. Mansour. *J. Coord. Chem.*, **66**, 1118 (2013).
- [62] M. Layek, M. Ghosh, M. Fleck, R. Saha, D. Bandyopadhyay. *J. Coord. Chem.*, **67**, 3371 (2014).
- [63] M. Amirnasr, R. Sadeghi Erami, K. Mereiter, K. Schenk Joß, S. Meghdadi, S. Abbasi. *J. Coord. Chem.*, **68**, 616 (2015).
- [64] D. Shoba, S. Periandy, M. Karabacak, S. Ramalingam. *Spectrochim Acta. Part A*, **83**, 540 (2012).
- [65] K. Fukui. *Science*, **218**, 747 (1982).
- [66] C.J. Brabec, N.S. Sariciftci, J.C. Hummelen. *Adv. Funct. Mater.*, **11**, 15 (2001).
- [67] R.C. Maurya, B.A. Malik, J.M. Mir, P.K. Vishwakarma, D.K. Rajak, N. Jain. *J. Mol. Struct.* **1099**, 266 (2015).
- [68] R.G. Pearson. *Acc. Chem. Res.*, **26**, 250 (1993).
- [69] Y. Sun, X. Chen, L. Sun, X. Guo, W. Lu. *J. Chem. Phys. Lett.*, **381**, 397 (2003).
- [70] O. Christiansen, J. Gauss, J.F. Stanton. *J. Chem. Phys. Lett.*, **305**, 147 (1999).
- [71] R.S. Mulliken. *J. Chem. Phys.*, **23**, 1833 (1995).
- [72] F. Billes, A. Holmgren, H. Mikosch. *Vib. Spectrosc.*, **53**, 296 (2010).
- [73] E. Scrocco, J. Tomasi. *Adv. Quantum Chem.*, **11**, 115 (1979).
- [74] F.J. Luque, J.M. López, M. Orozco. *Theor. Chem. Acc.*, **103**, 343 (2000).
- [75] N. Okulik, A.H. Jubert. *J. Mol. Des.*, **4**, 17 (2005).
- [76] P. Politzer, J.S. Murray. *Theor. Chem. Acc.*, **108**, 134 (2002).
- [77] P. Politzer, D.G. Truhlar. *Chemical Applications of Atomic and Molecular Electrostatic Potentials*, Plenum, New York (1981).
- [78] K.S. Lee, E.O. Price, J.E. Land. *J. Am. Chem. Soc.*, **78**, 1325 (1950).
- [79] Z.D. Hill, P. MacCarthy. *J. Chem. Educ.*, **63**, 162 (1986).
- [80] M. Lamsa, T. Kuokkanen. *J. Phys. Org. Chem.*, **9**, 21 (1996).
- [81] N.J. Rose, R.S. Drago. *J. Am. Chem. Soc.*, **81**, 6138 (1959).
- [82] H.A. Benesi, J.H. Hilderbrand. *J. Am. Chem. Soc.*, **71**, 2703 (1949).